



Fluorescent “on–off–on” sensor based on N, P co-doped carbon nanoparticles for specific detection of Fe³⁺ and ascorbic acid

Follow this and additional works at: <https://www.jfda-online.com/journal>

 Part of the [Food Science Commons](#), [Medicinal Chemistry and Pharmaceutics Commons](#), [Pharmacology Commons](#), and the [Toxicology Commons](#)



This work is licensed under a [Creative Commons Attribution-Noncommercial-No Derivative Works 4.0 License](#).

Recommended Citation

Li, Li; Zhang, Ming; Liu, Xiang; and Zhu, Shaoqing (2024) "Fluorescent “on–off–on” sensor based on N, P co-doped carbon nanoparticles for specific detection of Fe³⁺ and ascorbic acid," *Journal of Food and Drug Analysis*: Vol. 32 : Iss. 4 , Article 12.

Available at: <https://doi.org/10.38212/2224-6614.3533>

This Original Article is brought to you for free and open access by Journal of Food and Drug Analysis. It has been accepted for inclusion in Journal of Food and Drug Analysis by an authorized editor of Journal of Food and Drug Analysis.

Fluorescent “on–off–on” sensor based on N, P co-doped carbon nanoparticles for specific detection of Fe³⁺ and ascorbic acid

Li Li ^{a,c,*}, Ming Zhang ^{b,1}, Xiang Liu ^a, Shaoqing Zhu ^a

^a Zhenjiang College, Zhenjiang, 212000, PR China

^b Jiangsu Vocational College of Agriculture and Forestry, Zhenjiang, 212000, PR China

^c Kangda College, Nanjing Medical University, Lianyungang, 222000, PR China

Abstract

Ascorbic acid (AA) is used as a food additive for its antibacterial and antioxidant properties. However, excessive intake of AA is harmful to humans. Therefore, the detection of Fe³⁺ and AA is generally recognized to be meaningful. In this work, a one-step hydrothermal tactics is developed for the preparing nitrogen and phosphorus co-doped carbon nanoparticles (N, P-CNPs) by using sucrose and ammonium orthophosphate as raw materials. The N, P-CNPs not only exhibited an enhanced fluorescent efficiency with a relatively high quantum yield up to 28%, but also showed satisfactory stability, water solubility and photostability. The fluorescence of N, P-CNPs can be effectively quenched by Fe³⁺ by a combination of inner filter effect (IFE) and static quenching and recovered upon the addition of AA due to the easy conversion of Fe³⁺ to reduced states Fe²⁺ by AA. Therefore, a turn-off-on fluorescent sensing strategy can be constructed for sequential detection of Fe³⁺ and AA with detection limits of 0.03 μM and 6 nM with the corresponding linear ranges of 0.05–500 μM and 0.01–500 μM respectively. The proposed fluorescent sensor exhibits excellent sensing performance and has been applied to the determination of Fe³⁺ in tap water and the analyses of AA in canned fruit soup with satisfactory results. Therefore, this fluorescent sensor expressed high potential in water quality monitoring, and could be further used to be a tool for practical food additives detection.

Keywords: Ascorbic acid, Co-doped carbon nanoparticles, Fe³⁺, On-off-on fluorescent nano-sensor, Sucrose

1. Introduction

Fluorescent carbon nanoparticles (CNPs) have attracted tremendous attention in many areas, due to their unique combination of many distinct merits, such as high photostability, excellent biocompatibility, low cytotoxicity, good water solubility, anti-photobleaching, good dispersibility and chemical inertness [1–4]. However, the pristine CNPs have a high density of defect states, which lead to their low fluorescence efficiency and selectivity. Fortunately, heteroatom doping has been proven as an efficient way to improve the fluorescent efficiency of CNPs [5,6]. Co-doping with heteroatoms may introduce more active sites to CNPs,

which would broaden applications of CNPs in sensing.

In recent years, fluorescent detection technology has been extensively applied in environmental and food analysis [7]. In particular, nanomaterial-based “on-off-on” fluorescent sensors have received much attention because of their high sensitivity, wide detection range, strong anti-interference ability, and flexible design [8].

Fe³⁺ is one of the heavy metal ions which is toxic to fish and other aquatic organisms [9], it could cause many environmental problems. Excess and shortage of some metal ions like Fe³⁺ ions in drinking water away from permissible levels can cause severe health threat. So quantitative and

Received 29 February 2024; accepted 24 September 2024.
Available online 15 December 2024

* Corresponding author at: Zhenjiang College, Zhenjiang, 212000, PR China.
E-mail address: hrzmlily@163.com (L. Li).

¹ Authors contribute equally to this article.

<https://doi.org/10.38212/2224-6614.3533>

2224-6614/© 2024 Taiwan Food and Drug Administration. This is an open access article under the CC-BY-NC-ND license (<http://creativecommons.org/licenses/by-nc-nd/4.0/>).

accurate determination of iron ions in drinking water and water environment play a vital role in maintaining environment and human health [10]. Simultaneously, food industries utilize widely ascorbic acid (AA) as a food additive to prevent the changes of food color and taste based on its antioxidant property. So far, AA has been widely used as a food additive in foods such as fruit juice, soft drinks, and canned fruits [11]. However, inadequate intake will lead to the symptoms of scurvy, gingival bleeding, while excess intake will result in urinary stone, diarrhoea and stomach convulsion. The Food and Nutrition Board of National Academies recommends the average amount of AA for male and female a day is 90 mg and 75 mg respectively, and the maximum daily intake for an adult is about 2000 mg [12]. Several fluorescence sensing detection methods have been developed for the simultaneous detection of Fe^{3+} and AA [12–15]. However, the above methods have drawbacks such as the complexity of the process of synthesizing fluorescence sensing materials, the low fluorescence quantum yield of the synthesized fluorescent materials and narrow linear range. Therefore, there is an urgent need to develop fluorescent sensing materials with simple and green synthesis methods and high fluorescence quantum yields for the simultaneous detection of Fe^{3+} and AA for environmental sanitation and food safety.

To date, in the above reported fluorescence sensing method for simultaneous detection of Fe^{3+} and AA, several raw materials have been developed for synthesis of co-doped CNPs, including beer [16], chitosan and κ -carrageenan [17], oleic acid, L-cystine and citric acid [18], DL-malic acid and levofloxacin [19], L-Cys and 1-amino-2-naphthol-4-sulfonic acid (ANSA) [20], citric acid and thiourea [21], ammonium citrate tribasic and vitamin B₁ [22], etc. However, to the best of our knowledge, the fluorescent nano-sensing system for fast and simultaneous detection of Fe^{3+} and AA based on the use of sucrose has not been previously studied. In

the present study, we designed a simple and low-cost hydrothermal method for the synthesis of nitrogen and phosphorus co-doped carbon nanoparticles (N, P-CNPs) using sucrose and ammonium orthophosphate as raw materials. The fluorescence of N, P-CNPs could be efficiently quenched by Fe^{3+} by a combination of inner filter effect (IFE) and static quenching. When introduced AA into the sensing system, Fe^{3+} was reduced to Fe^{2+} along with the fluorescence recovery of N, P-CNPs. Based on the phenomenon, a fluorescence switchable sensor was developed to selectively detect Fe^{3+} and AA in real samples. The detail of this strategy is performed in Scheme 1, and the detection results are better than other reported fluorescent probes.

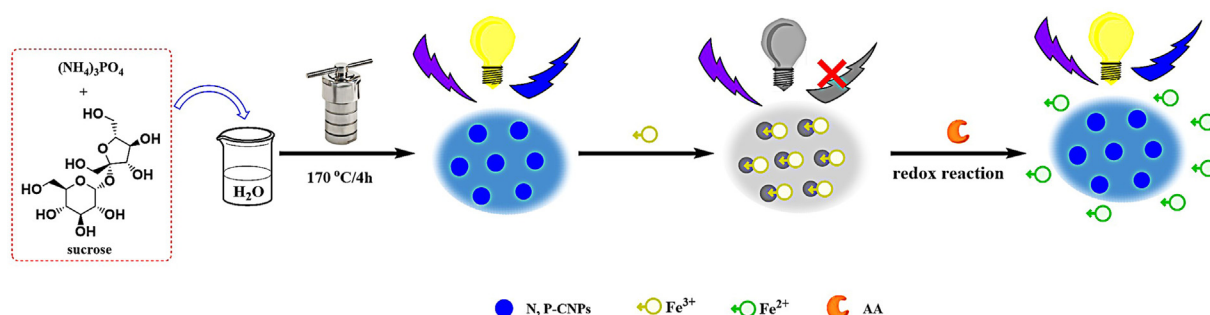
2. Experimental section

2.1. Materials and reagents

Sucrose, ammonium orthophosphate, FeCl_3 , carboxymethylcellulose sodium and citric acid were purchased from Sinopharm Chemical Reagent Co., Ltd (P. R. China). Sodium alginate, gluconolactone, malic acid, acesulfame, sodium gluconate were, lactose, tartaric acid, dextrin, and vitamin B₁ were obtained from Shanghai Macklin Biochemical Technology Co., Ltd (P. R. China). NaCl was purchased from Nanjing Chemical Reagent Co., Ltd (P. R. China). All the chemicals were of analytical grade, and directly used as received without any further purification. The canned coconut was purchased from a local supermarket in Jiangsu province, P. R. China. All the solutions were prepared with ultrapure water, which was obtained from a Milli-Q purification system (Millipore, United States).

2.2. Apparatus

Transmission Electron Microscope (TEM) images were obtained from a HT7800 transmission electron



Scheme 1. One-step hydrothermal synthesis of N, P-CNPs from sucrose and “turn-off-on” fluorescence sensing of Fe^{3+} and AA using N, P-CNPs.

microscope (Hitachi Limited, Japan). X-ray photoelectron spectroscopy (XPS) was measured on a AXIS-ULTRA DLD electron spectrometer (Kratos Analytical Limited, UK). Fourier transform infrared spectra (FT-IR) was recorded on Nicolet iS50 FT-IR spectrophotometer (Thermo Fisher Scientific, USA) from 400 to 4000 cm^{-1} . X-ray diffraction (XRD) patterns were acquired on a D8 Advance X-ray diffractometer (Bruker, Germany). The data was collected from $2\theta = 5\text{--}80^\circ$ at a scan rate of 5°min^{-1} . A fluorescence spectrophotometer RF-6000 (Shimadzu, Japan) with xenon lamp as the source of excitation was used to record the emission fluorescence spectra. Ultraviolet-visible (UV-vis) absorption spectra was recorded on a BioMate 3S UV-vis spectrophotometer (Thermo Fisher Scientific, USA). The fluorescence lifetimes were measured with a FLS1000 steady/transient fluorescence spectrometer (Edinburgh Instruments, UK) with excitation at 365 nm. All optical measurements were recorded under stable ambient conditions.

2.3. Synthesis of N, P-CNPs

In a typical procedure, 0.34 g of sucrose and 0.60 g of ammonium orthophosphate were added to 25 mL ultra-pure water and stirred to dissolve them completely. Then the mixture solution was transferred to a 50 mL Teflon-lined stainless autoclave and heated to 170°C for 4 h. After that, the crude product was cooled to room temperature. The reaction product was then centrifuged for 10 min at 12,000 rpm to remove nonfluorescent deposits. Afterwards, the resultant light yellow solution was collected, filtered with a microporous membrane ($0.22 \mu\text{m}$), and finally dialyzed for 48 h through a dialysis membrane (MWCO = 1000) in ultrapure water. The final product was further dried under freeze drying to obtain N, P-CNPs.

2.4. Determination of fluorescence quantum yields (QY)

The QY of the as-prepared N, P-CNPs was measured by a relative method with quinine sulfate (dispersed in $0.1 \text{ mol}\cdot\text{L}^{-1} \text{H}_2\text{SO}_4$, $QY_{ref} = 54\%$) as the reference. The emission ($\lambda_{ex} = 350 \text{ nm}$) and UV-Vis spectra of quinine sulfate and N, P-CNPs were measured, respectively. The QY was calculated using the following formula [23]:

$$QY = QY_{ref} \times \frac{\eta^2}{\eta_{ref}^2} \times \frac{I}{I_{ref}} \times \frac{A_{ref}}{A} \quad (1)$$

Among the formula, QY, I, and A are the quantum yield, integrated fluorescence (FL) intensity, optical absorbance, respectively. η_{ref} is refractive index of quinine sulfate. η is the refractive index of the sample. Both ' η ' and ' η_{ref} ' are 1.33. The subscript '*ref*' corresponds to the standard. A is the absorbance at 350 nm.

2.5. Fluorescence detection of Fe^{3+}

The as-prepared solid products of N, P-CNPs were dissolved in ultrapure water to make a $100 \mu\text{g}\cdot\text{mL}^{-1}$ solution of N, P-CNPs. The quenching effect of Fe^{3+} on the FL intensity of N, P-CNPs was conducted as follows: 10 μL of the N, P-CNPs solution was diluted into 1890 μL of ultrapure water, in which 100 μL of the Fe^{3+} solutions at varying concentrations were added, and the final solution volume was made up to 2.0 mL, and the mixture was shaken thoroughly. After mixing and leaving under reaction for 1 min, the FL intensity at 442 nm was measured under excitation wavelength at 322 nm. All experiments were repeated three times.

2.6. Fluorescent detection of AA

A series of working standard solution with different concentrations of AA were prepared by diluting a concentrated standard solution of AA with ultrapure water. Thereafter, in a typical process, 10 μL of N, P-CNPs solution ($100 \mu\text{g}\cdot\text{mL}^{-1}$) and 100 μL of ferric chloride solution (1000 μM) were mixed, then 1800 μL of AA working standard solutions with different concentrations were added into the mixture solution (N, P-CNPs/ Fe^{3+}), and then were diluted to 2 mL with ultrapure water, and the mixture was shaken thoroughly. After incubation for 1 min at room temperature, the FL intensity of the solutions was recorded on a fluorescence spectroscopy at the excitation wavelength of 322 nm. A calibration graph was derived on the basis of the relationship between the concentration of AA and the fluorescence enhancement efficiency $(F_t - F_s)/F_s$, where F_s and F_t represent the FL intensity of N, P-CNPs/ Fe^{3+} system in the absence/presence of AA. All samples for fluorescence measurements were performed in triplicate, and the data were recorded as a mean. All experiments were conducted under a stable room temperature.

2.7. Sample analysis under actual conditions

Local tap water samples from Jiangsu Province in China were collected, then filtered with a $0.22 \mu\text{m}$

microfiltration membrane to remove impurities. After the pretreatments, 100 μL of the samples, 10 μL of 100 $\mu\text{g}\cdot\text{mL}^{-1}$ N, P-CNPs solution and 1890 μL of ultrapure water were mixed to detect the Fe^{3+} concentration. The FL intensity was measured under the excitation of 322 nm.

The canned coconut collected from a local supermarket was used for actual sample analysis. The procedure was as follows: the canned coconut soup samples were centrifuged at 10,000 r/min for 20 min, and next, the supernate was filtered with 0.22 μm filter to remove the impurities. The determination of AA in canned coconut soup was consistent with the above-mentioned standard solution of AA.

3. Results and discussion

3.1. Optimizing preparation conditions of N, P-CNPs

To obtain N, P-CNPs with optimal fluorescence, the raw material ratio, preparation temperature and reaction time of the hydrothermal process were optimized, and the results were depicted in Fig. 1. In Fig. 1A, as the mole ratio of sucrose to ammonium orthophosphate decreased, the fluorescence intensity raised first and then decreased. When the ratio is 1:4, the FL intensity of N, P-CNPs is maximum, so 1:4 was the optimal molar ratio. Furthermore, the preparation temperature and reaction time were optimized. As exhibited in Fig. 1B and 1C, the highest FL intensity was observed at 170 $^{\circ}\text{C}$ for 4 h, and the further increases in synthetic temperatures and times would lead to the prominently decreased FL intensity of N, P-CNPs. Consequently, the above reaction conditions were adopted for the subsequent preparation of N, P-CNPs.

3.2. Characterization of the N, P-CNPs

The size and morphology of N, P-CNPs were investigated using TEM. TEM images are displayed in Fig. 2, which shows the spherical shape and good dispersion of N, P-CNPs in the solution. The size distribution of N, P-CNPs is depicted in Fig. 2 by randomly counting about 100 N, P-CNPs particles from TEM image. The particle size is 2–33 nm, and the average particle size is 15 nm.

The XRD pattern of the N, P-CNPs shows a broad diffraction peak centered at around 21.6 $^{\circ}$ (Fig. 3A), illustrating that the N, P-CNPs has an obvious amorphous carbon structure. These results demonstrate that the N, P-CNPs have the structure of spherical-like and amorphous carbon, possessing excellent dispersing performance in ultrapure water. On the other hand, as shown in FTIR spectrum (Fig. 3B), there was stretching vibration peak located at 3222 cm^{-1} ascribed to $-\text{OH}/-\text{NH}_2$ group. The bands at 2972 and 2925 cm^{-1} belong to C–H stretching vibration. The sharp absorption peaks at 1632 cm^{-1} was assigned to the stretching vibration of C=O band. The peaks at 1452 cm^{-1} and 1400 cm^{-1} were assigned to the in-plane flexural vibration O–H

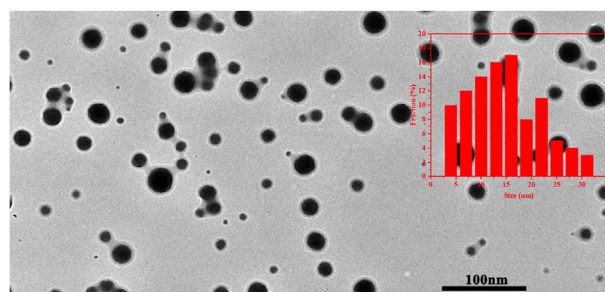


Fig. 2. TEM image of N, P-CNPs (top inset: diameter size distribution histogram by taking 100 particles into account).

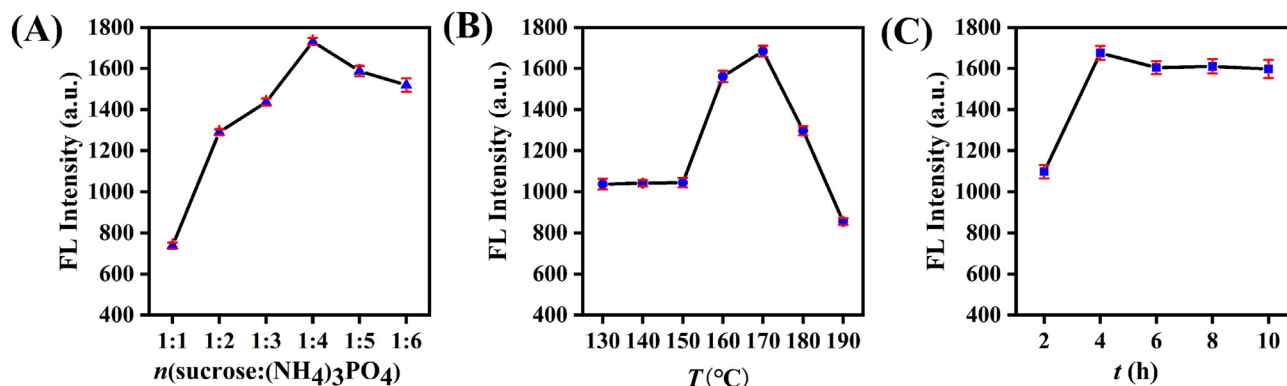


Fig. 1. Fluorescence spectra ($\lambda_{\text{ex}} = 322 \text{ nm}$) of the N, P-CNPs synthesized with (A) various raw material ratio at (B) different reaction temperature for (C) different reaction time.

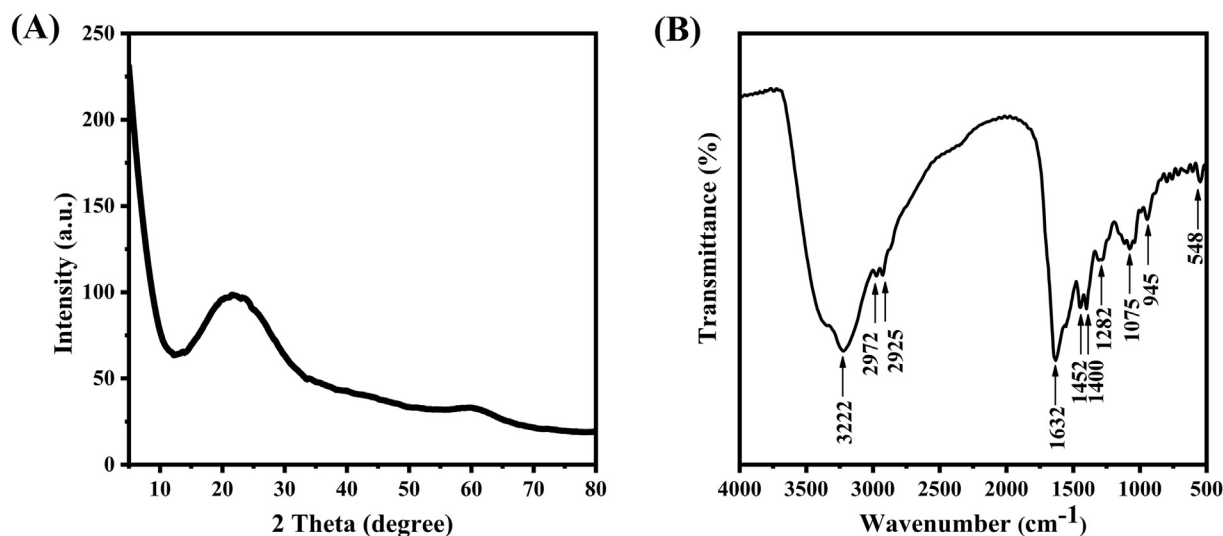


Fig. 3. (A) XRD of N, P-CNPs. (B) FTIR spectrum of N, P-CNPs.

bond and C–H band. The characteristic peaks located at 1282 cm^{-1} , 1075 cm^{-1} , 945 cm^{-1} and 548 cm^{-1} were attributed to C–O, P–O–C, P–O–H and PO_4^{3-} , respectively. All these results also proved the successful doping of nitrogen and phosphorus atoms in N, P-CNPs. These results also indicated that there were many functional groups such as –COOH, –OH, –NH₂ and – PO_4^{3-} on the surface of N, P-CNPs, which were conducive to the high hydrophilicity and stability in aqueous solution.

Further confirmation of the surface chemistry and the chemical composition of the prepared N, P-CNPs was conducted using high resolution X-ray photoelectron spectroscopy (XPS). Fig. 4 displays the survey and deconvoluted spectra of each identified elements. The analysis results show that the atomic content percentages of C, N, O and P in the prepared N, P-CNPs are 70.0%, 10.2%, 18.2% and 1.6%, respectively. The result indicates that the synthetic CNPs are effectively doped by N and P. The survey spectra (Fig. 4A) shows four major peaks corresponding to O1s ($\sim 532\text{ eV}$), N1s ($\sim 400\text{ eV}$), C1s ($\sim 285\text{ eV}$), and P2p ($\sim 134\text{ eV}$). The C1s spectrum (Fig. 4B) could be resolved into peaks at 285.8 and 284.9 eV, and be equivalent to C–N/C–P, and C–C/C=C. P2p spectrum (Fig. 4C) confirms the presence of P–O (134.8 eV), P–C/P–N (133.8 eV) and P=O (133.0 eV). The N1s spectrum (Fig. 4D) revealed the existence of N–C/N–H and pyridinic N (=NH–) locating at 400.8 eV and 399.5 eV. The O1s peak (Fig. 4E) was divided into C–OH/C–O–C (532.2 eV) and C=O (530.7 eV). The XPS measurement confirmed that the functional groups depicted on N,

P-CNPs were in accordance with the consequences of FTIR.

3.3. Optical performance of the N, P-CNPs

The spectral properties including UV–vis absorption spectra, fluorescence spectra, and fluorescence QY were investigated. As can be seen from the black line in Fig. 5A, the N, P-CNPs have a absorption peak at 270 nm, which is ascribed to the $n-\pi^*$ of C=O bond. The optimal excitation (λ_{ex} , red line) and emission (λ_{em} , blue line) peaks are situated at 322 nm and 442 nm, respectively. Meanwhile, the aqueous solution of N, P-CNPs can emit bright blue fluorescence under UV light of 365 nm, and it appeared transparent and pale yellow under daylight (inset of Fig. 5A). To further study the optical properties of N, P-CNPs, the emission spectras of N, P-CNPs were measured at various excitation wavelengths ranging from 282 to 362 nm, and the result is shown in Fig. 5B. It is noticed that the emission peak almost remains at the similar positions when the excitation wavelength increases from 282 to 362 nm, exhibiting an excitation-independent wavelength behavior. Besides, the strongest emission intensity of N, P-CNPs was achieved when they were excited at 322 nm. Therefore, the excitation wavelength of 322 nm was used for the following experiment. Using quinine sulfate as the reference (with QY 0.54 in $0.1\text{ mol}\cdot\text{L}^{-1}\text{ H}_2\text{SO}_4$), the relative fluorescence QY of the N, P-CNPs in aqueous solution at room temperature was calculated as 28% at an excitation wavelength of 350 nm. The reason for

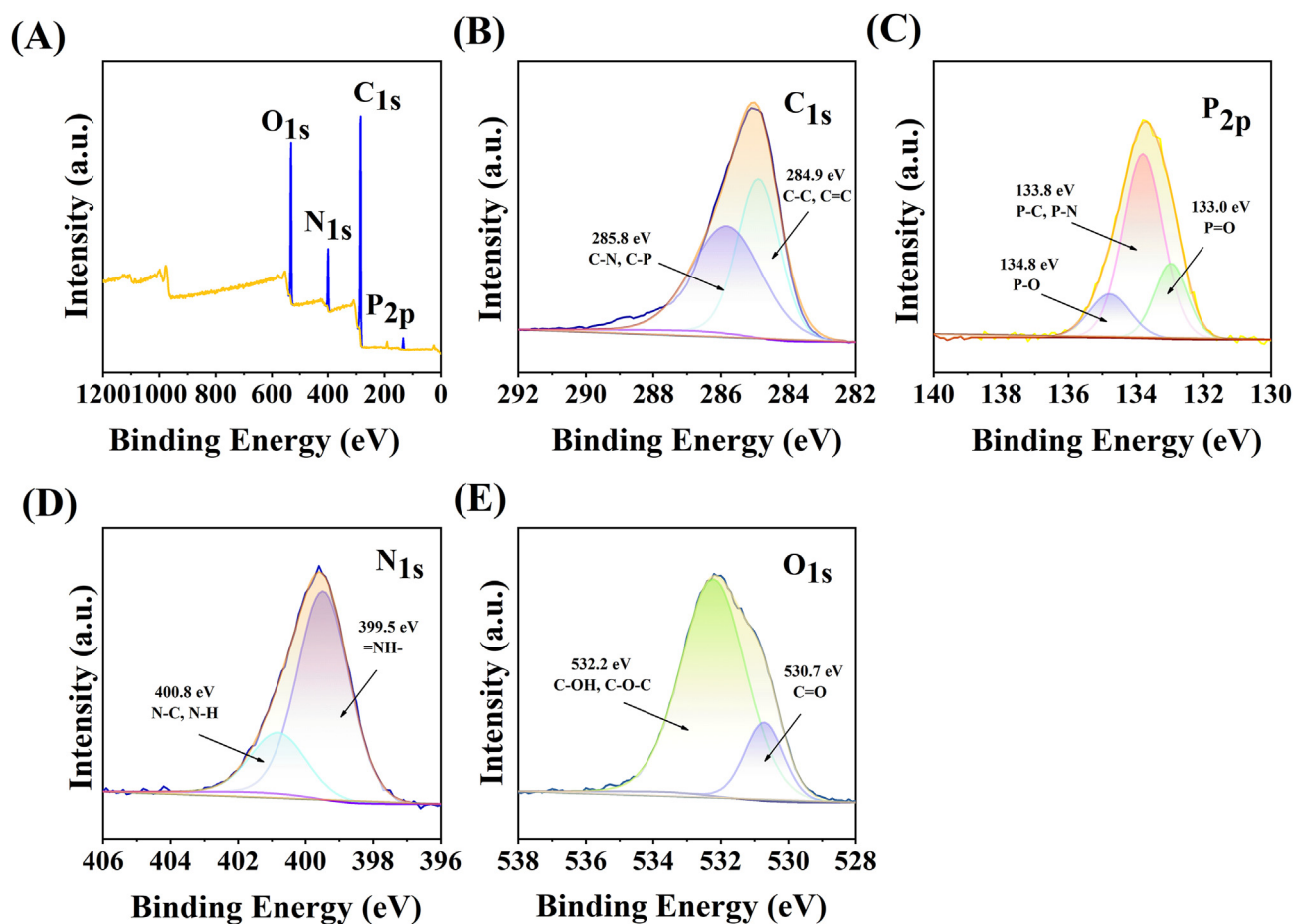


Fig. 4. (A) XPS survey scan, (B) C1s XPS, (C) P2p XPS, (D) N1s XPS, (E) O1s XPS of N, P-CNPs.

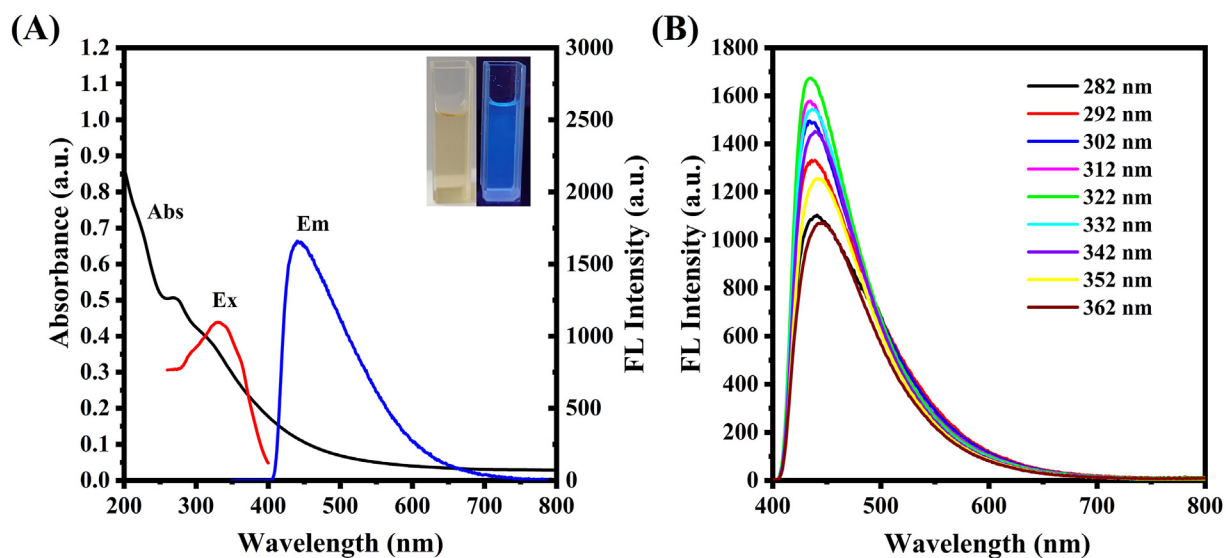


Fig. 5. (A) UV-Vis absorption (black), excitation (red) and emission (blue) spectra of N, P-CNPs. [Inset: photographs of N, P-CNPs in visible-light (left) and under UV-light ex 365 nm (right)]. (B) The emission spectra of the N, P-CNPs under various excitation wavelength.

this higher QY may be due to the synergistic effect of doped N and P atoms.

3.4. Fluorescence stability of N, P-CNPs

Generally, the fluorescence stability is considered as an especially significant factor for their potential applications. Hence, the fluorescence performances of the N, P-CNPs solution encountering different conditions are examined in detail. First, the influence of ionic strength on the fluorescence stability of the N, P-CNPs was investigated. As can be seen from the fluorescence data, the FL intensity shows almost no obvious differences with the increase in the surrounding ionic strengths by regulating the concentrations of NaCl from 0 to 2 mol·L⁻¹ (Fig. 6A). Second, UV exposure on the fluorescence stability of the N, P-CNPs was investigated. No serious fluorescence bleaching was observed after

continuous UV-light irradiation for 60 min (Fig. 6B). Third, Fig. 6C shows the stable FL intensity of the N, P-CNPs maintained in a refrigerator at 4 °C for four months. This proved that the N, P-CNPs were inert. Fourth, the pH effect on the FL intensity of N, P-CNPs had been studied. The FL intensity of N, P-CNPs could remain stable when the pH value of phosphate buffer [24] was from 4 to 10, and it was not much different from the FL intensity in ultra-pure water (Fig. 6D). In addition, the effect of pH value of phosphate buffer on the detection of Fe³⁺ was observed. As depicted in Fig. 6E, the difference values of the FL intensity of the N, P-CNPs before and after adding 500 μM of Fe³⁺ were basically constant with the raise of pH value. Additionally, after adding 600 μM of AA, the fluorescence recovering effect of N, P-CNPs/Fe³⁺ system will also reach relatively well between pH 4 and 7, which is basically consistent with the experimental results in

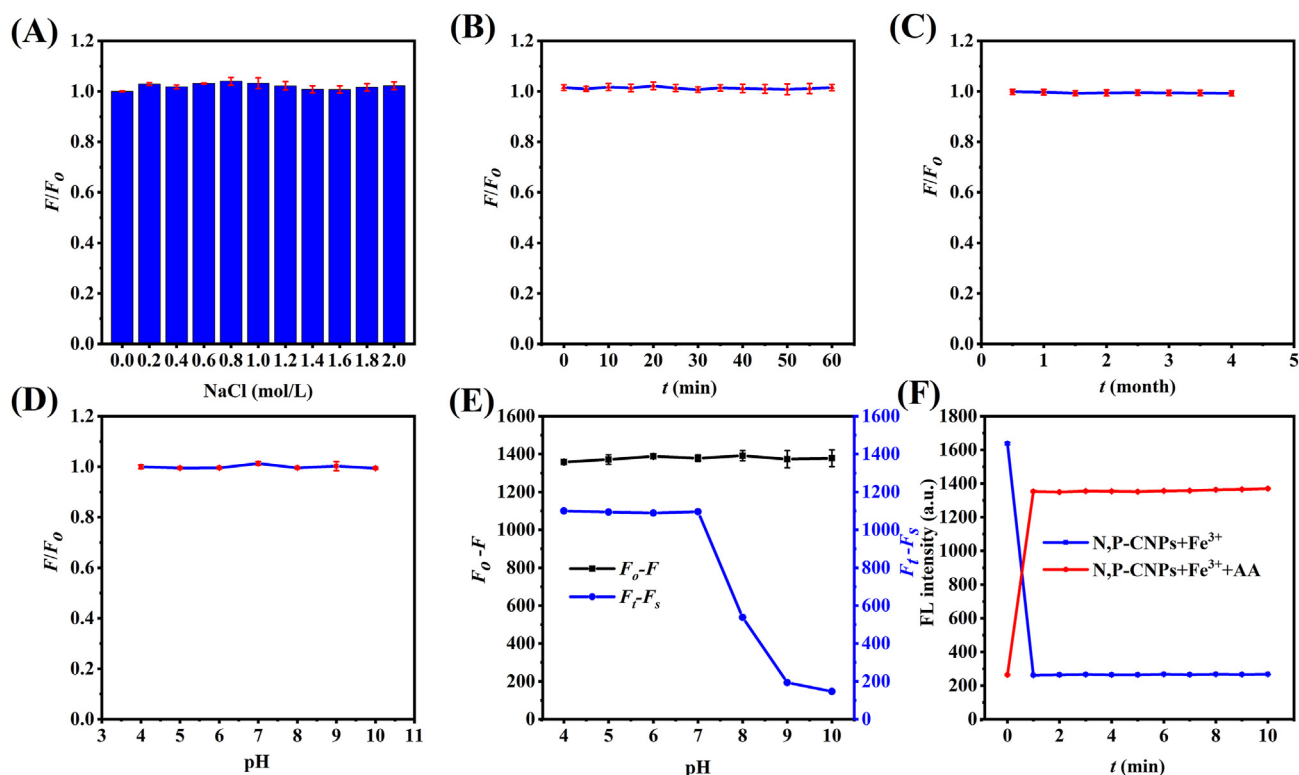


Fig. 6. (A) Effect of ionic strengths on the FL intensity of N, P-CNPs (ionic strengths were controlled by various concentrations of NaCl in aqueous solution, F_0 represents the FL intensity of the blank sample, and F represents the FL intensity of the sample following the incorporation of NaCl solutions with different concentrations at 442 nm). (B) Effect of time intervals of irradiation with a UV lamp on FL intensity of N, P-CNPs (F_0 represents the FL intensity of the original sample, F represents the FL intensity of the sample exposed to light for different time). (C) Effect of storage time on the FL intensity of the N, P-CNPs maintained in a refrigerator at 4 °C (F_0 represents the FL intensity of the original sample, F represents the FL intensity of the sample stored for different time). (D) Effect of pH on the FL intensity of N, P-CNPs (F_0 represents the FL intensity of the blank sample, F represents the FL intensity of the sample following the incorporation of phosphate buffer solutions with different pH values at 442 nm). (E) Effect of pH on the FL intensity of N, P-CNPs in phosphate buffer solutions with different pH values after adding Fe³⁺ and AA (F_0-F) represents the difference value of the FL intensity of the N, P-CNPs before and after adding 500 μM of Fe³⁺ (black line), (F_f-F_s) represents the difference value of the FL intensity of the N, P-CNPs/Fe³⁺ system before and after adding 600 μM of AA (blue line)). (F) The FL intensity of N, P-CNPs after adding 500 μM of Fe³⁺ (blue line) and 500 μM of Fe³⁺+600 μM of AA (red line).

ultrapure water. However, the fluorescence recovering effect of N, P-CNPs/ Fe^{3+} system is poor under alkaline conditions. Therefore, all experiments were carried out in ultrapure water without adjusting pH value of solution [16,25]. Finally, the incubation time (quenching and recovery time) was investigated to evaluate the fluorescence sensing response time to Fe^{3+} and AA, and the curves of FL intensity versus incubation time were shown in Fig. 6F. The fluorescence of N, P-CNPs was quenched to minimum value after adding 500 μM of Fe^{3+} within 1 min and remained relatively constant for 10 min, indicating that Fe^{3+} quenching was rapid and stable. In addition, the FL intensity at 442 nm was rapidly restored within 1 min following the addition of 600 μM AA, with a recovery rate of 83%. After 10 min, the FL intensity changed little, indicating that the FL intensity recovered quickly and stably after adding AA. So, the probe could fill the rapid detection of Fe^{3+} and AA.

3.5. Selectivity study of the N, P-CNPs-based probe for analyzing Fe^{3+} and AA

The anti-interference effect of as-fabricated probe is one of the important parameters in determining

its feasibility in real detection. First of all, it was studied whether other interferences affect the fluorescence of N, P-CNPs scientifically. As shown in Fig. 7A, when 900 μM of Fe^{3+} was added into N, P-CNPs solutions (100 $\mu\text{g}\cdot\text{mL}^{-1}$), it was evident that the quenching efficiencies $(F_0-F)/F_0$ enhanced significantly. However, there is no obvious fluorescence quenching effects when 4500 μM of other interferences including Na^+ , K^+ , Fe^{2+} , Cu^{2+} , Zn^{2+} , Ca^{2+} , Pb^{2+} , Mg^{2+} , Co^{2+} , Ni^{2+} , Al^{3+} , sodium alginate, gluconolactone, malic acid, sucrose, carboxymethylcellulose sodium, acesulfame, sodium gluconate, lactose and tartaric acid (except citric acid and dextrin are 900 μM , and Vitamin B₁ is 1800 μM) were added to N, P-CNPs. Moreover, to further determine the selectivity of N, P-CNPs for Fe^{3+} , other interferences were added to a solution of N, P-CNPs containing Fe^{3+} in 900 μM of concentration. The results revealed that the N, P-CNPs had high selectivity for the detection of Fe^{3+} and can be used as a good fluorescent sensor for Fe^{3+} detection.

The selectivity of the N, P-CNPs/ Fe^{3+} system for the detection of AA was explored in the presence of other possible interferences, which included citric acid, sodium alginate, gluconolactone, malic acid, sucrose, carboxymethylcellulose sodium, acesulfame, sodium

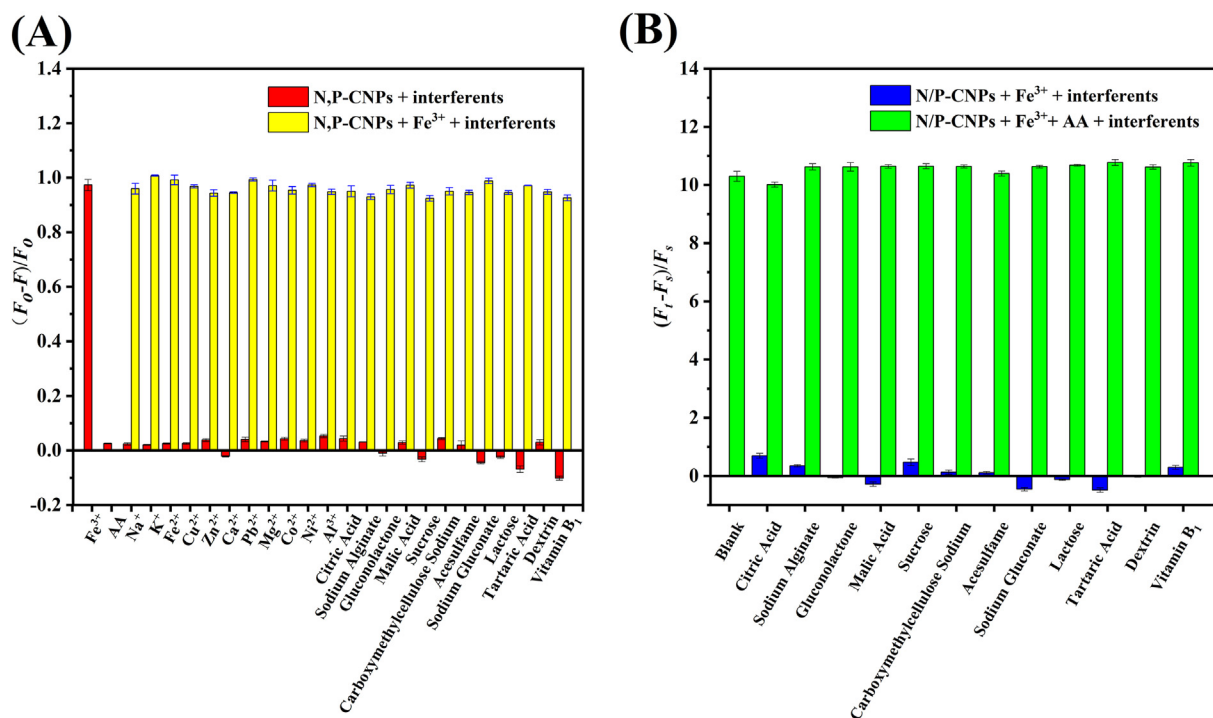


Fig. 7. (A) Selectivity of the N, P-CNPs for Fe^{3+} (interferents are 5-fold concentration of Fe^{3+} , except citric acid and dextrin are in equal concentration of Fe^{3+} and Vitamin B₁ is 2-fold concentration of Fe^{3+}), where F_0 and F were the FL intensity of the N, P-CNPs in the absence and presence of Fe^{3+} respectively. (B) Selectivity of N, P-CNPs/ Fe^{3+} system for AA (interferents are 5-fold concentration of AA, except citric acid and dextrin are in equal concentration of AA and Vitamin B₁ is 2-fold concentration of AA), where F_s and F_i were the FL intensity of the N, P-CNPs/ Fe^{3+} system in the absence and presence of AA respectively.

gluconate, lactose, tartaric acid, dextrin, and Vitamin B₁. As shown in Fig. 7B, only AA induced a significant fluorescence restoration of N, P-CNPs, in sharp contrast, other interferences did not cause significant changes of FL intensity. More importantly, the recovery of N, P-CNPs/Fe³⁺ FL intensity by AA did not interfere by other coexisting small interfering substances. Therefore, the N, P-CNPs/Fe³⁺ sensor possesses excellent selectivity and reliability toward AA quantification.

3.6. Sensitivity study of the N, P-CNPs-based probe for analyzing Fe³⁺ and AA

To further study the sensitivity of the N, P-CNPs for Fe³⁺, the fluorescence of the N, P-CNPs was investigated by adding different concentrations of Fe³⁺ (0–1000 μM) under the optimum conditions. Fig. 8A shows that as the concentration of Fe³⁺ increased, the FL intensity of the N, P-CNPs gradually decreased. The relationship between the F₀/F of the N, P-CNPs and the concentration of Fe³⁺ is shown in Fig. 8B, where a good linear relationship was obtained in the range from 0.05 μM to 500 μM with the correlation coefficient (R²) of 0.9940. The linear equation was F₀/

F = 0.0092C + 1.3017, where C is the concentration of Fe³⁺, and F₀ and F are the fluorescence intensities of N, P-CNPs at 442 nm in the absence and presence of Fe³⁺, respectively. The limit of detection for Fe³⁺ was calculated to be 0.03 μM based on the equation LOD = 3σ/S, where σ is the standard deviation of the blank samples and S is the slope of the standard curve [26–28]. According to the Standards for Drinking Water Quality of China National Standards (GB 5749-2022) and the Drinking Water Standards and Health Advisories of U.S. Environmental Protection Agency (EPA), the threshold limit of Fe³⁺ content in water is 0.3 mg/L (5.37 μM) [29,30]. Additionally, the maximum concentration of Fe³⁺ in drinking water regulated by the World Health Organization (WHO) is 2 mg/L (35.81 μM) [31]. These threshold limits are much higher than the detection limit of Fe³⁺ established by this method, so the application of this method can accurately detect whether the content of Fe³⁺ in drinking water exceeds the limit requirements prescribed by China National Standards, EPA and WHO. Moreover, the sensitivity of N, P-CNPs/Fe³⁺ sensor system to AA was investigated via the fluorescence emission spectra by adding various concentrations of AA. With the addition of AA from 0 μM to 1300 μM, the

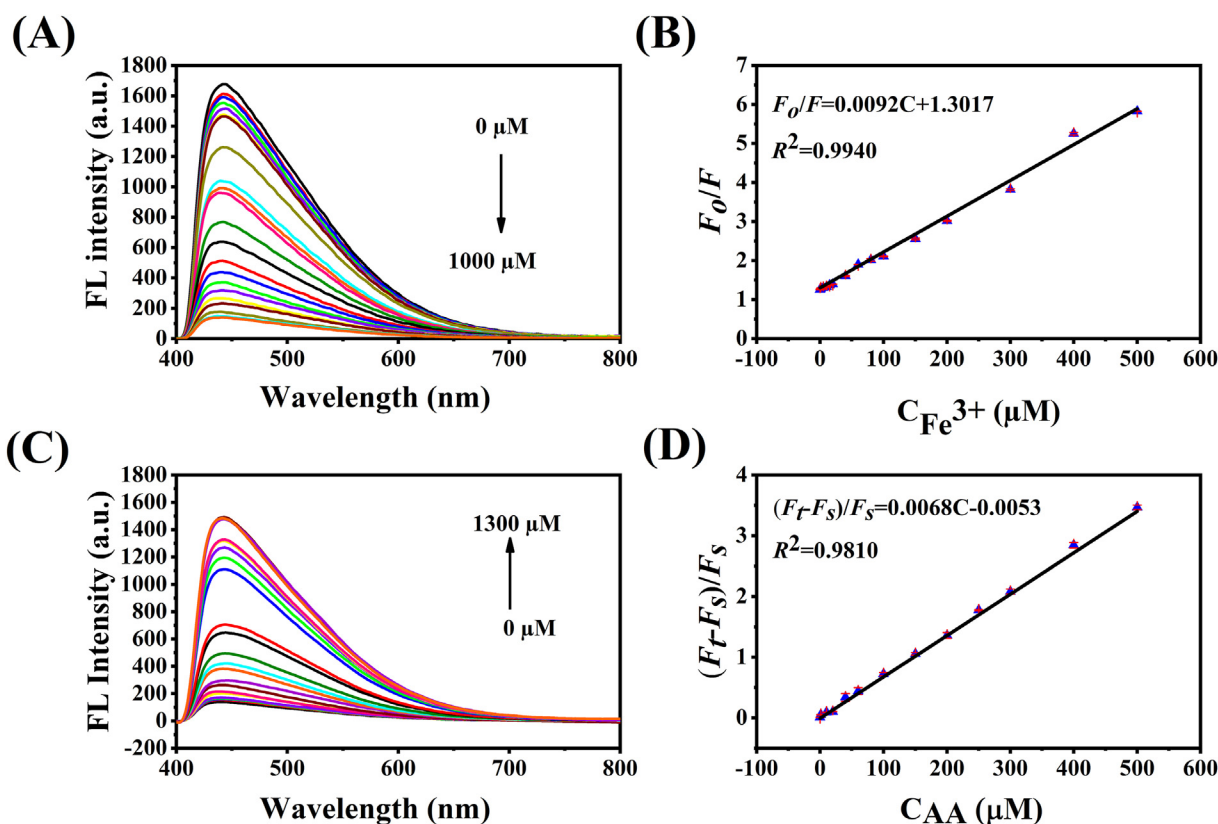


Fig. 8. (A) Fluorescence emission spectra of N, P-CNPs with different concentrations of Fe³⁺ (from top to down: 0–1000 μM). (B) Calibration plot of F₀/F versus concentration of Fe³⁺ (0.05–500 μM) (C) Fluorescence emission spectra of N, P-CNPs/Fe³⁺ system with different concentrations of AA (from down to top: 0–1300 μM). (D) Calibration plot of (F_t - F_s)/F_s versus concentration of AA (0.01–500 μM).

FL intensity of N, P-CNPs/Fe³⁺ emission peak at 442 nm gradually increased (Fig. 8C). The relationship curve of the fluorescence enhancement ratio $(F_t - F_s)/F_s$ versus AA concentration (0.01–500 μM) was displayed in Fig. 8D, where F_s is the fluorescence emission intensity of N, P-CNPs/Fe³⁺, F_t is fluorescence emission intensity of N, P-CNPs/Fe³⁺ recovered by AA. The linear equation was $(F_t - F_s)/F_s = 0.0068C - 0.0053$ with linear correlation coefficient (R^2) of 0.9810, where C is the concentration of AA. The detection limit for AA was 6 nM calculated according to the equation $LOD = 3\sigma/S$ [26–28].

Compared with other chosen probes in the literature (Table 1), the advantages of the fluorescent N, P-CNPs probe developed in this study include its simple operation, rapid detection and determination, ease of use, low cost, relatively wide linear range, lower detection limit, high sensitivity, high selectivity, and applicability to real samples.

3.7. Quenching mechanism study of the N, P-CNPs–Fe³⁺ system

To investigate the quenching mechanism between N, P-CNPs and Fe³⁺, the UV–vis absorption spectra of Fe³⁺ and the fluorescence spectra of the N, P-CNPs were studied. Fig. 9A shows that there was obvious overlap between the excitation spectrum of the N, P-CNPs and the absorption spectrum of Fe³⁺, revealing that the excitation energy of N, P-CNPs can be competitively absorbed by Fe³⁺, resulting in the quenching of the fluorescence of N, P-CNPs. As the IFE usually occurs when the excitation spectrum or emission spectrum of the donor has obvious overlap with the absorption spectrum of the acceptor [32–34], Fe³⁺ can quench the fluorescence of the N, P-CNPs probably via the IFE. Besides, as shown in Fig. 9B, when Fe³⁺ was added into N, P-CNPs solution, the characteristic absorption peak of Fe³⁺ at ca. 250–350 nm were emerged and increased with the increasing of the Fe³⁺ concentration, and no offset of the peak position and no new peaks were observed, demonstrating no new substance was generated. Fig. 8A illustrates that the fluorescence intensity at 442 nm of the N, P-CNPs decreases with the increasing of Fe³⁺, and this phenomenon maybe caused by this reason: a stronger absorption peak of Fe³⁺ at ca. 250–350 nm absorbed the excitation energy of N, P-CNPs at 322 nm. The fact further confirmed the IFE mechanism in the presence of Fe³⁺ [35,36].

In principle, fluorescence lifetime measurement is the most definitive method to distinguish dynamic and static quenching processes. In light of this, fluorescence lifetime quenching analysis is carried out to confirm the nature of quenching. The

fluorescence lifetimes of N, P-CNPs with and without Fe³⁺ were tested, the average fluorescence lifetimes of N, P-CNPs and N, P-CNPs/Fe³⁺ were 6.71 ns and 6.22 ns, respectively (Fig. 9C), and the fluorescence lifetimes changed little after the addition of Fe³⁺, indicating the static quenching process [12,32,33]. In addition, the Stern-Volmer equation (2) was applied to study the quenching process [32,33].

$$F_0/F = 1 + K_{sv}[Q] = 1 + k_q\tau_0[Q] \quad (2)$$

Among the formula, F_0 and F are the FL intensity of N, P-CNPs without and with Fe³⁺, respectively. K_{sv} refers to the Stern-Volmer quenching constant. k_q is the bimolecular quenching constant. $[Q]$ refers to the Fe³⁺ contents. τ_0 refers to the fluorescence lifetime of N, P-CNPs (6.71 ns). Herein, the linear equation was $F_0/F = 0.0092[Q] + 1.3017$ ($R^2 = 0.9940$) (Fig. 8B). In the light of this linear equation, K_{sv} and k_q were carried out to be $9.2 \times 10^3 \text{ L} \cdot \text{mol}^{-1}$ and $1.37 \times 10^{12} \text{ L} \cdot \text{mol}^{-1} \text{ s}^{-1}$. The k_q value was significantly greater than the maximum scatter collision quenching constant ($2 \times 10^{10} \text{ L} \cdot \text{mol}^{-1} \text{ s}^{-1}$), revealing that the other mechanism was static quenching [32–34]. Ultimately, it was perceived that the detection mechanism for Fe³⁺ in this study was the result of IFE and static quenching effect.

After adding AA to N, P-CNPs, there was no obvious change in the intensity and peak position of the fluorescence spectra of N, P-CNPs, indicating no interaction between N, P-CNPs and AA. However, the FL intensity was dramatically reduced after adding Fe³⁺, and then recovered upon addition of AA (Fig. 9D), which may be due to the special redox reaction between Fe³⁺ and AA [17,32]. Fe³⁺ is reduced to Fe²⁺, thus eliminating IFE as well as regaining the fluorescence of N, P-CNPs. In order to verify the formation of Fe²⁺, 1, 10-phenanthroline (Fe²⁺ specific indicator) was added to the solutions of N, P-CNPs/Fe³⁺ and N, P-CNPs/Fe³⁺+AA separately, and the UV-vis absorption spectra were shown in Fig. 9E. The N, P-CNPs/Fe³⁺+AA in the presence of 1,10-phenanthroline (0.15%) presented an obvious absorption at ~510 nm compared to N, P-CNPs/Fe³⁺, which can be attributed to the orange-red complex of Fe²⁺ with 1,10-phenanthroline. The UV-vis absorption spectra further verified the existence of Fe²⁺ in the system of N, P-CNPs/Fe³⁺+AA [37,38]. Thus, the N, P-CNPs, could be used as a switchable turn “on-off-on” fluorescent nanoprobe for Fe³⁺ and AA.

3.8. Detection of Fe³⁺ in real samples

To verify the viability of this fluorescent probe, tap water from Jiangsu Province in China was collected

Table 1. Comparison of several typical fluorescent probes for the detection of Fe³⁺ and AA.

Probe	QY (%)	Detection range of Fe ³⁺	Detection limit of Fe ³⁺	Detected Sample for Fe ³⁺	Detection range of AA	Detection limit of AA	Detected Sample for AA	Response time (min)	References
Graphite-like carbon nitride nanosheets (g-C ₃ N ₄ NNs)	9.6	0.05–30 μM	0.018 μM	lake	0.2–112.5 μM	0.086 μM	human serum	5 (AA)	[12]
Nitrogen doped graphene quantum dots (N-GQDs)	N/A ^a	0.5–50 μM	N/A ^a	tap water	1–60 μM	N/A ^a	human urine samples	N/A ^a	[15]
Nitrogen and sulfur co-doped carbon dots (N, S-CDs)	59.31	1–100 μM	57 nM	N/A ^a	0.5–90 μM	38 nM	N/A ^a	10 (Fe ³⁺)	[17]
N,S-CDs	23.7	0–10 μM	36.6 nM	water samples	0–30 μM	102.5 nM	vitamin C tablets	20 (Fe ³⁺); 1 (AA)	[18]
N,S-CDs	24.6	5.00–105 μM	0.10 μM	wolfberry, red jujube	4.97–54.8 μM	2.4 nM	orange	1 (Fe ³⁺); 1 (AA)	[20]
Cu/Mn:carbon quantum dots (CQDs)	28.35	0–80 μM	16 nM	tap water, drinking water	0–80 μM	46 nM	tap water, drinking water	3 (Fe ³⁺); 3 (AA)	[21]
N,S-CDs	26	0–100 μM	0.13 μM	tap, bore, and pond water	0.5–100 μM	0.2 μM	human urine and serum	2 (Fe ³⁺); 10 (AA)	[23]
Nitrogen-doped carbon quantum dots (N-CQDs)	22	6–100 μM	3 μM	lake, drinking water, and tap water	10–100 μM	1.8 μM	vitamin tablets	1 (Fe ³⁺); 6 (AA)	[24]
Tea-CDs	7.1	53.5–267.9 μM	0.15 μM	tap water	0.2–0.8 mM	19.78 μM	effervescent tablets	1 (Fe ³⁺); 1 (AA)	[25]
Myrica rubra-based N-doped carbon dots (MN-CDs)	23.4	1–1000 mM	0.3 μM	environmental waters	0.1–1000 mM	0.03 μM	pharmaceutical tablets and fruit juice samples	2 (Fe ³⁺); 10 (AA)	[32]
Green-emitting CDs (G-CDs)	27.2	0.05–10.0 μM	13.7 nM	well, river and bottled mineral waters	0.2–11.0 μM	82.0 nM	human urine samples	2 (Fe ³⁺); 15 (AA)	[39]
Nitrogen and boron-incorporated carbon dots (NBCDs)	5.13	0–0.7 mM	7.50 μM	acid rain	0–1.5 mM	7.72 μM	N/A ^a	2 (Fe ³⁺); 30 (AA)	[40]
Ni-Metal Organic Framework functionalized Nitrogen-doped carbon quantum dots (Ni-MOF-NCDs)	N/A ^a	0.029–8.0 μg/mL	0.0098 μg/mL	tap water	0.263–18.0 μg/mL	0.0876 μg/mL	oranges, vitamin C effervescent tablets and vitamin C tablets	5 (Fe ³⁺); 10 (AA)	[41]
CDs	47.2	0.03–15.0 μM	10.2 nM	river water	0.1–25.0 μM	54.3 nM	apple, tomato	2 (Fe ³⁺); 2 (AA)	[42]
GSH-capped gold nano-clusters (GSH-AuNCs)	N/A ^a	0.7–180.0 μM	0.07 μM	tap water	0.5–120.0 μM	0.03 μM	vitamin C effervescent tablets and kiwi juice	0.5 (Fe ³⁺); 18 (AA)	[43]
Nitrogen-doped carbon dots (N-CDs)	19.3	25–200 μM	58.82 nM	tap water	25–300 μM	0.236 μM	orange, purple grape, kiwi	2 (AA)	[44]
CDs	18.53	10 nM–50 μM	5 nM	water samples and human serum	0–200 μM	5 μM	N/A ^a	1 (Fe ³⁺); 12 (AA)	[45]
N, P-CNPs	28	0.05–500 μM	0.03 μM	tap water	0.01–500 μM	6 nM	canned fruit soup	1 (Fe ³⁺); 1 (AA)	present work

^a N/A: Not available.

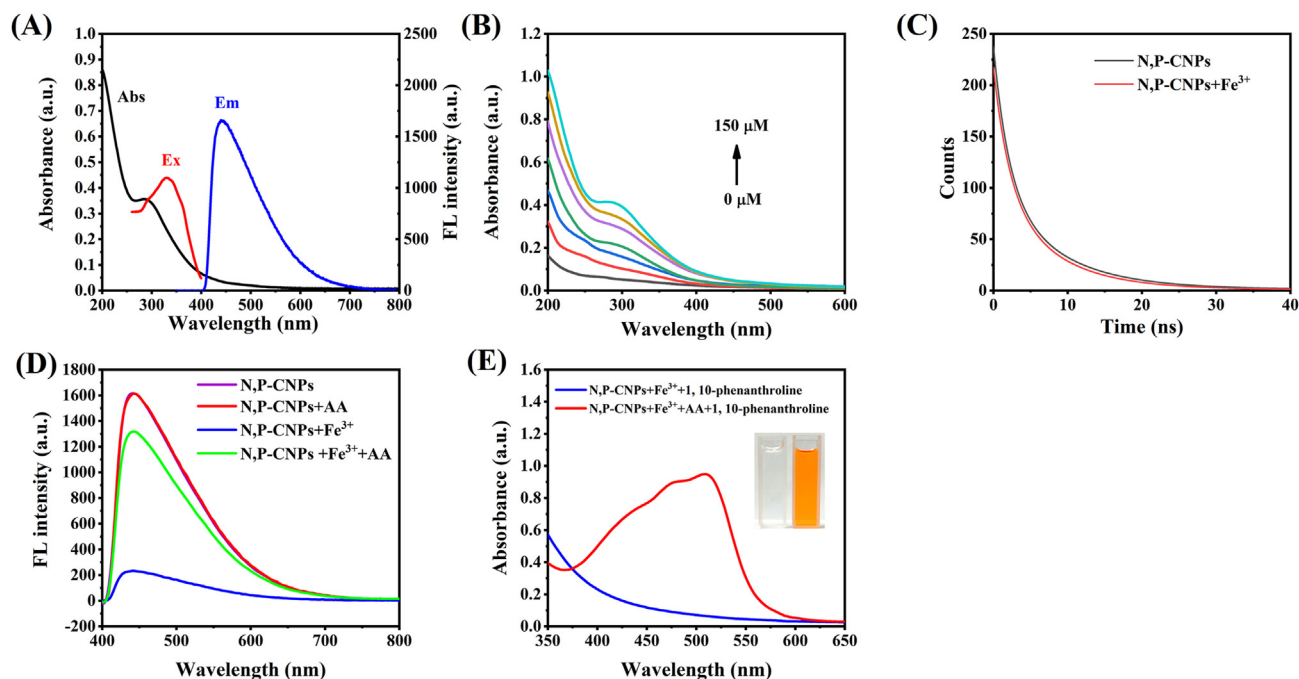


Fig. 9. (A) UV-vis absorption of Fe³⁺ (black line), as well as excitation (red line) and emission (blue line) spectra of the N, P-CNPs. (B) The UV-vis absorption spectra of Fe³⁺ at 0.375 μg/mL of N, P-CNPs in ultrapure water. The concentrations of Fe³⁺ are: 0–150 μM. (C) Fluorescence decay of N, P-CNPs and N, P-CNPs + Fe³⁺. (D) Fluorescence emission spectra of N, P-CNPs (purple line), N, P-CNPs + AA (red line), N, P-CNPs + Fe³⁺ (blue line), and N, P-CNPs + Fe³⁺ + AA (green line). (E) UV-vis absorption spectra of N, P-CNPs/Fe³⁺ and N, P-CNPs/Fe³⁺ + AA after adding 1, 10-phenanthroline (0.15%) separately. [Inset: photograph of N, P-CNPs/Fe³⁺ (left) and N, P-CNPs/Fe³⁺ + AA (right) aqueous solutions with the presence of 1, 10-phenanthroline (0.15%) under visual light, respectively].

and used to test the reliability and efficiency of the proposed system. The tap water samples were collected and spiked with certain concentrations known of Fe³⁺ and the results of the determination have been presented in Table 2. Spiked recoveries were clearly in the range of 98.6%–100.8% and the relative standard deviation (RSD) was less than 2.00%. From these results, it can be summarized that the N, P-CNPs had good performance in real samples and they can be used to effectively detect Fe³⁺ in water samples.

3.9. Detection of AA in canned coconut soup

Meanwhile, this method also tested the content of AA in canned coconut soup. The canned coconut

Table 2. Determination of Fe³⁺ in actual water samples with the proposed method (n = 3).

Sample	Original (μM)	Added (μM)	Found (μM)	Recovery (%)	RSD ^b (%)
Tap water	ND ^a	45.00	44.92 ± 0.6	99.8	1.33
		105.00	105.79 ± 1.26	100.8	1.20
		175.00	172.52 ± 0.96	98.6	0.56

^a ND: non-detectable or below the limit of detection (0.02 μM).

^b RSD: relative standard deviation.

Table 3. Determination of AA in canned coconut soup samples with the proposed method (n = 3).

Sample	Original (μM)	Added (μM)	Found (μM)	Recovery (%)	RSD ^a (%)
Canned coconut soup	141.49 ± 1.32	50.00	188.04 ± 3.53	98.2	1.88
		100.00	251.63 ± 3.53	104.2	1.40
		150.00	298.78 ± 2.41	102.5	0.81

^a RSD: relative standard deviation.

soup was pretreated by centrifugation, filtration and dilution to reduce the interference of pulp and large granular viscous matrix. As revealed in Table 3, the AA content detected in canned coconut soup was 141.49 μmol/L, the spike recoveries for AA determination ranged from 98.2% to 104.2%, with RSD less than 2.00%. The results verified the reliability and practicality of this method.

4. Conclusions

In summary, we developed a simple and low-cost strategy to fabricate N, P-CNPs by hydrothermal treatment of sucrose and ammonium orthophosphate. The obtained N, P-CNPs were successfully applied as “on–off–on” fluorescent probe for the

sequential detection of Fe³⁺ and AA in real water and canned coconut soup samples. The newly developed N, P-CNPs-based switch probe has the advantages of simple detection condition, inexpensive instrument, rapid response, wide linear range, low detection limit and excellent selectivity towards various interfering chemicals, and thus shows great potential in real applications.

Conflicts of interest

There are no conflicts to declare.

Acknowledgements

This work was supported by the Jiangsu Overseas Research & Training Program for University Prominent Young & Middle-aged Teachers and Presidents Fund, the Qing Lan Project Fund of Jiangsu Province, Jiangsu Higher Vocational College Engineering Research Center of Green Energy and Low Carbon Materials, The Natural Science Foundation of the Jiangsu Higher Education Institutions of China (22KJB360019), the Key Program of the Science and Technology Funds of Zhenjiang College (No. GZZD202304), and Initial Scientific Research Fund for Talents in Zhenjiang College (No. 4153230008/013).

References

- [1] Yoo D, Park Y, Cheon B, Park MH. Carbon dots as an effective fluorescent sensing platform for metal ion detection. *Nanoscale Res Lett* 2019;14:272.
- [2] Gao PL, Xie ZG, Zheng M. Small nanoparticles bring big prospect: the synthesis, modification, photoluminescence and sensing applications of carbon dots. *Chin Chem Lett* 2022;33:1659–72.
- [3] Pichardo-Molina JL, Cardoso-Avila PE, Flores-Villavicencio LL, Gomez-Ortiz NM, Rodriguez-Rivera MA. Fluorescent carbon nanoparticles synthesized from bovine serum albumin nanoparticles. *Int J Biol Macromol* 2020;142:724–31.
- [4] Zuo PL, Zhang JY, Zhou YQ, Xie NJ, Xiao DL. Spontaneous formation of fluorescent carbon nanoparticles in glutaraldehyde solution and their fluorescence mechanism. *J Fluoresc* 2021;31:509–16.
- [5] Guillermo Redondo-Fernandez, Cigales Canga Jesus, Ana Soldado, Ruiz Encinar Jorge, Costa-Fernandez Jose M. Functionalized heteroatom-doped carbon dots for biomedical applications: a review. *Anal Chim Acta* 2023;1284:341874.
- [6] Chen BB, Liu ML, Li CM, Huang CZ. Fluorescent carbon dots functionalization. *Adv Colloid Interface Sci* 2019;270:165–90.
- [7] Gong ZY, Chan HT, Chen QL, Chen HB. Application of nanotechnology in analysis and removal of heavy metals in food and water resources. *Nanomaterials* 2021;11:1792.
- [8] He HY, Sun DW, Wu ZH, Pu HB, Wei QY. On-off-on fluorescent nanosensing: materials, detection strategies and recent food applications. *Trends Food Sci Technol* 2022;119:243–56.
- [9] Wang MR, Liu ML, Nong SL, Song WZ, Zhang XP, Shen S, et al. Highly luminescent nucleoside-based N, P-doped carbon dots for sensitive detection of ions and bioimaging. *Front Chem* 2022;10:906806.
- [10] Li ZW, Tan B, Wu ZF, Huang XY. A robust strontium coordination polymer with selective and sensitive fluorescence sensing ability for Fe³⁺ ions. *Materials* 2023;16:577.
- [11] Pei KL, Xu JY, Wu D, Qi L, Ma LY, Zhang RW, et al. A fluorescent dual-emitting platform for fluorescent "turn-on" ratiometric detection of ascorbic acid in beverages utilizing luminol-embedded iron-based metal-organic frameworks. *Food Chem* 2024;434:137417.
- [12] Guo XR, Yue GQ, Huang JZ, Liu C, Zeng Q, Wang LS. Label-free simultaneous analysis of Fe(III) and ascorbic acid using fluorescence switching of ultrathin graphitic carbon nitride nanosheets. *ACS Appl Mater Inter* 2018;10:26118–27.
- [13] Hu CS, Zhu YM, Zhao XF. On-off-on nanosensors of carbon quantum dots derived from coal tar pitch for the detection of Cu²⁺, Fe³⁺, and L-ascorbic acid. *Spectrochim Acta* 2021;250:119325.
- [14] Jia HP, Li ZP, Wang FX, Lu RH, Zhang SB, Zhang ZQ. Facile synthesis of NH₂-MIL-53(AI)/RhB as a dual-emitting on-off-on probe for the detection of Fe³⁺ and L-ascorbic acid. *Microchem J* 2023;188:108464.
- [15] Xu HB, Zhou SH, Fang WB, Fan YZ. Synthesis of N-doped graphene quantum dots from bulk N-doped carbon nanofiber film for fluorescence detection of Fe³⁺ and ascorbic acid. *Fuller Nanotub Carbon Nanostructures* 2021;29:218–26.
- [16] Li XY, Wang C, Li P, Sun XY, Shao ZY, Xia J, et al. Beer-derived nitrogen, phosphorus co-doped carbon quantum dots: highly selective on-off-on fluorescent probes for the detection of ascorbic acid in fruits. *Food Chem* 2023;409:135243.
- [17] Xu JY, Wang YS, Sun LL, Qi Q, Zhao XH. Chitosan and κ-carrageenan-derived nitrogen and sulfur co-doped carbon dots "on-off-on" fluorescent probe for sequential detection of Fe³⁺ and ascorbic acid. *Int J Biol Macromol* 2021;191:1221–7.
- [18] Nie YJ, Guo JQ, Deng YH, Weng W. Synthesis and application of fluorescent N,S co-doped carbon dots based on on-off-on quenching mode for the collaboration detection of iron ions and ascorbic acid. *J Saudi Chem Soc* 2020;24:865–73.
- [19] Zhao Y, Zhu XX, Liu L, Duan ZQ, Liu YP, Zhang WY, et al. One-step synthesis of nitrogen/fluorine co-doped carbon dots for use in ferric ions and ascorbic acid detection. *Nanomaterials* 2022;12:2377.
- [20] Du Q, Zhao XY, Mei XP, Zhao YQ, Dong C, Li JF. A sensitive sensor based on carbon dots for the determination of Fe³⁺ and ascorbic acid in foods. *Anal Methods* 2024;16:939–49.
- [21] Latief U, Ul Islam S, Khan MS. Rare-earth free solid-state fluorescent carbon-quantum dots: multi-color emission and its application as optical dual-mode sensor. *J Alloys Compd* 2023;941:168985.
- [22] Wang RN, Wang Y, Zhao N, Zhao HQ, Yuan XC, Zhao LS. Nitrogen and sulfur co-doped carbon quantum dots for detecting Fe³⁺, ascorbic acid and alkaline phosphatase activities. *J Fluoresc* 2023. <https://doi.org/10.1007/s10895-023-03539-y>.
- [23] Bandi R, Devulapalli NP, Dadigala R, Gangapuram BR, Guttena V. Facile conversion of toxic cigarette butts to N,S-codoped carbon dots and their application in fluorescent film, security ink, bioimaging, sensing and logic gate operation. *ACS Omega* 2018;3:13454–66.
- [24] Gu L, Zhang JR, Yang GX, Tang YY, Zhang X, Huang XY, et al. Green preparation of carbon quantum dots with wolfberry as on-off-on nanosensors for the detection of Fe³⁺ and L-ascorbic acid. *Food Chem* 2022;376:131898.
- [25] Chen K, Qing WX, Hu WP, Lu MH, Wang Y, Liu XH. On-off-on fluorescent carbon dots from waste tea: their properties, antioxidant and selective detection of CrO₄²⁻, Fe³⁺, ascorbic acid and L-cysteine in real samples. *Spectrochim Acta Mol Biomol Spectrosc* 2019;213:228–34.
- [26] Lai WQ, Guo JQ, Zheng N, Nie YJ, Ye SA, Tang DP. Selective determination of 2,4,6-trinitrophenol by using a novel carbon

- nanoparticles as a fluorescent probe in real sample. *Anal Bioanal Chem* 2020;412:3083–90.
- [27] Zhan YC, Chiu CP, Chen YC. Using lanthanide ions as magnetic and sensing probes for the detection of tetracycline from complex samples. *J Food Drug Anal* 2023;31:371–80.
- [28] Lo KM, Lin YS, Liou JW, Chiu TC, Hu CC. Electrochemically synthesized green fluorescent carbon dots for quantitation of hypochlorite and carbendazim. *J Food Drug Anal* 2023;31:244–53.
- [29] Standardization Administration of China. Standards for drinking water quality. In: China national Standards (No. GB 5749-2022). Beijing, China: Standardization Administration of China; 2022.
- [30] U.S. Environmental Protection Agency. 2018 edition of the drinking water standards and health Advisories. Washington, DC, USA: U.S. Environmental Protection Agency; 2018.
- [31] World Health Organization. Guidelines for drinking-water quality, fourth edition incorporating the first and second addenda. Geneva, Switzerland: World Health Organization; 2022.
- [32] Fan R, Xiang JX, Zhou PP, Mei H, Li YY, Wang HL, et al. Reuse of waste *Myrica rubra* for green synthesis of nitrogen-doped carbon dots as an "on-off-on" fluorescent probe for Fe^{3+} and ascorbic acid detection. *Ecotoxicology* 2022;233:113350.
- [33] Sudewi S, Chabib L, Zulfajri M, Gedda G, Huang GG. Polyvinylpyrrolidone-passivated fluorescent iron oxide quantum dots for turn-off detection of tetracycline in biological fluids. *J Food Drug Anal* 2023;31:177–93.
- [34] Laddha H, Yadav P, Jain Y, Sharma M, Reza M, Agarwal M, et al. One-pot microwave-assisted synthesis of blue emissive multifunctional N-S-P co-doped carbon dots as a nanoprobe for sequential detection of Cr(VI) and ascorbic acid in real samples, fluorescent ink and logic gate operation. *J Mol Liq* 2022;346:117088.
- [35] Zhang QX, Sun Y, Liu ML, Liu Y. Selective detection of Fe^{3+} ions based on fluorescence MXene quantum dots via a mechanism integrating electron transfer and inner filter effect. *Nanoscale* 2020;12:1826–32.
- [36] Song SM, Liang F, Li ML, Du FF, Dong WJ, Gong XJ, et al. A label-free nano-probe for sequential and quantitative determination of Cr(VI) and ascorbic acid in real samples based on S and N dual-doped carbon dots. *Spectrochim Acta* 2019;215:58–68.
- [37] Chen SF, Song Y, Li Y, Liu YL, Su XG, Ma Q. A facile photoluminescence modulated nanosensor based on nitrogen-doped graphene quantum dots for sulfite detection. *New J Chem* 2015;39:8114–20.
- [38] Luo XL, Zhang WG, Han Y, Chen XM, Zhu L, Tang WZ, et al. N, S co-doped carbon dots based fluorescent "on-off-on" sensor for determination of ascorbic acid in common fruits. *Food Chem* 2018;258:214–21.
- [39] Shamsipur M, Molaei K, Molaabasi F, Alipour M, Alizadeh N, Hosseinkhani S, et al. Facile preparation and characterization of new green emitting carbon dots for sensitive and selective off/on detection of Fe^{3+} ion and ascorbic acid in water and urine samples and intracellular imaging in living cells. *Talanta* 2018;183:122–30.
- [40] Wang LL, Chung JS, Hur SH. Nitrogen and boron-incorporated carbon dots for the sequential sensing of ferric ions and ascorbic acid sensitively and selectively. *Dyes Pigments* 2019;171:107752.
- [41] Xu OW, Wan SY, Yang J, Song HY, Dong LZ, Xia J. Ni-MOF functionalized carbon dots with fluorescence and adsorption performance for rapid detection of Fe (III) and ascorbic acid. *J Fluoresc* 2022;32:1743–54.
- [42] Tu JQ, Yang XY, Liu HP, Chen P, Liu K, Gao J. A 'on-off-on' fluorescent probe for sensitive detection of Fe^{3+} and ascorbic acid by cross-linking agent protected carbon dots. *Int J Environ Anal Chem* 2022;102:243–53.
- [43] Dong WJ, Yu JY, Gong XJ, Liang WT, Fan L, Dong C. A turn-off-on near-infrared photoluminescence sensor for sequential detection of Fe^{3+} and ascorbic acid based on glutathione-capped gold nanoclusters. *Spectrochim Acta Mol Biomol Spectrosc* 2021;247:119085.
- [44] Du FF, Gong XJ, Lu WJ, Liu Y, Gao YF, Shuang SM, et al. Bright-green-emissive nitrogen-doped carbon dots as a nanoprobe for bifunctional sensing, its logic gate operation and cellular imaging. *Talanta* 2018;179:554–62.
- [45] Wang M, Wan YY, Zhang KL, Fu QF, Wang LJ, Zeng J, et al. Green synthesis of carbon dots using the flowers of *Osmanthus fragrans* (Thunb.) Lour. as precursors: application in Fe^{3+} and ascorbic acid determination and cell imaging. *Anal and Bioanal* 2019;411. <https://doi.org/10.1007/s00216-019-01712-6>.